PCCP

PAPER

View Article Online
View Journal | View Issue

Cite this: *Phys. Chem. Chem. Phys.*, 2023, **25**, 2167

First principles study of layered scandium disulfide for use as Li-ion and beyond-Li-ion batteries†

Conor Jason Price, * Joe Pitfield, Edward Allery David Baker and Steven Paul Hepplestone *

The growing demand for high efficiency portable batteries has prompted a deeper exploration for alternative cathode materials. Due to low Earth abundance, scandium has not received much attention, however its low atomic mass makes it ideal for high gravimetric capacity electrodes. Here we have performed a comprehensive first-principles study to assess the performance of layered ScS_2 as a potential cathode for lithium-ion and beyond-lithium-ion batteries. We have explored the configuration space of ScS_2 and its intercalated compounds using a mix of machine learning and *ab initio* techniques, finding the ground state geometry to be layered in nature. This layered structure is found to have a high voltage, reaching above 4.5 V for Group I intercalants, ideal volume expansions below 10% for lithium and magnesium intercalation, is electronically conductive, and is ductile once intercalated. Of the intercalants considered, we find that lithium is the best choice for cathode applications, for which we have used a combination of thermodynamic phase diagrams, *ab intio* phonon calculations, and evaluation of the elastic tensor to conclude that ScS_2 possesses a reversible capacity of 182.99 mA h g^{-1}, on par with current state of the art cathode materials such as $LiCoO_2$, NMC, and NCA. Finally, we substitute foreign metal species into the ScS_2 material to determine their effect on key cathode properties, but find that these are overall detrimental to the performance of ScS_2. This does, however, highlight the potential for improvement if scandium were mixed into other layered systems such as the layered transition metal oxides.

Received 28th October 2022,
Accepted 9th December 2022

DOI: 10.1039/d2cp05055b

rsc.li/pccp

1 Introduction

As the demand for rechargeable batteries rises, the need for both better and a wider range of cathode materials rises with it. Whereas for anodes there are a wealth of materials available and the key challenge is competing with the abundance of hard carbons, for cathodes the range of materials is much lower with leading contenders being the phosphates,[1–3] the ubiquitous NMC and its variants,[4–9] and spinel oxides such as $LiMn_2O_4$.[10–13]

There has been some interest in the use of other intercalant species[14] due to the safety issues associated with lithium, its high cost of production, and the rising concern for the sustainability of lithium deposits. Other Group I elements[15–17] offer the same chemistry as lithium and so there is hope they would be able to match the performance of lithium. Alternatively, Group II elements have also been considered[18–20] as they possess two valence electrons and so the available charge transfer (and hence electrode energy storage) should in principle be twice that of the Group I elements.

For intercalation electrodes, layered materials such as the TMDCs,[21–23] NMC,[5,24] and the MXenes[25] are highly attractive as their van der Waals gaps allow for low diffusion barriers and hence fast intercalant transport. Recent works have started to note the potential of scandium, where the doping of metal oxides with scandium has been shown to increase particle size without affecting the crystal structure,[26] provide a comparable capacity whilst improve cycling stability,[26,27] and significantly lower the surface energy of nanoparticles.[28] With these clear structural and energetic improvements, as well as the fact that scandium is one of the lightest available metals, it raises the question as to how good scandium-based materials themselves would perform as electrode materials.

Transition metal oxides have been widely investigated and used for intercalation cathodes as they display high voltages and capacities. Lithium scandium dioxide ($LiScO_2$) has been experimentally verified to exist in only one form, a fractional cationic ordered rock-salt structure, with the $I4_1/amd$ space group.[29,30] This is similar to the anatase structure of TiO_2 but with lithium filling the voids. However, this material was found to have poor ionic conductivity, requiring substitutional doping with transition metals in place of the scandium atoms.[30] This lack of ionic conductivity prevents its exploitation as a cathode material. Alternative, layered structures have therefore been

Department of Physics, University of Exeter, Stocker Road, Exeter, EX4 4QL, UK. E-mail: cjp225@exeter.ac.uk, S.P.Hepplestone@exeter.ac.uk

† Electronic supplementary information (ESI) available. See DOI: https://doi.org/10.1039/d2cp05055b

considered,[31,32] but are unfeasible as the structure is energetically unfavourable compared to the rock-salt phase.

Layered sulfides are closely related to the oxides, and have the added benefit of being compatible with sulfide-electrolytes. Sulfide electrolytes are chemically unstable with high-voltage oxides due to the difference in electronegativity of oxygen and sulfur.[33] Thus, scandium-sulfide materials could offer the optimal properties for cathodes whilst allowing the use of sulfide-electrolytes. The bulk properties of the TMDC T- and H-phases of ScS_2 have been shown to be conducting,[34] however, the monolayer form of the H-phase is insulating.[34–36] For intercalation electrodes, the intercalated form of ScS_2 is of interest. $LiScS_2$, $NaScS_2$, and $KScS_2$ have all been synthesised,[37,38] and were found to have the layered α-$NaFeO_2$ structure with space group $R\bar{3}M$. Unfortunately, theoretical investigations of this structure have been limited to monolayers,[39,40] though these have suggested high capacities of over 400 mA h g^{-1} with lithium intercalation. However, monolayers are significantly more difficult to synthesise compared to their bulk counterpart, and do not provide an accurate representation of the dimensions of electrodes being utilised in functional devices. To the best of our knowledge there are currently no studies investigating the potential of bulk ScS_2 for electrodes, and so the questions of how well the bulk material would perform as an intercalation electrode remains.

In this work we explore the potential of intercalated ScS_2 compounds as a cathode material for lithium, sodium, potassium, and magnesium batteries using a range of theoretical techniques built upon first principles calculations. We explore the phase space of these materials to determine the lowest energy structures, determine the relevant properties for cathode performance, and evaluate their dynamic and thermodynamic stabilities to obtain a reversible intercalation capacity. Finally, we consider how the substitution of other metallic species in place of scandium affects these key properties for electrode applications.

2 Methods

2.1 First-principles methods

In this work, first principles techniques based on density functional theory were used to determine structural and energetic properties of layered scandium disulfide (ScS_2) intercalated with varying levels of lithium, sodium, potassium, and magnesium. These calculations were done using the Vienna Ab initio Simulation Package (VASP).[41–44] The valence electrons included for each species were Sc $3d^2$ $4s^1$, S $3s^2$ $3p^4$, Li $1s^2$ $2s^1$, Na $2p^6$ $3s^1$, K $3p^6$ $4s^1$, and Mg $2p^6$ $3s^2$. All other electrons were effectively contained within the used pseudopotentials. The projector augmented wave method[45] was used to describe the interaction between core and valence electrons, and a plane-wave basis set was used with an energy cutoff of 700 eV. van der Waals interactions have been addressed using the zero damping DFT-D3 method of Grimme.[46]

Three different phases of the ScS_2 structure were considered: the T-phase, the Hc-phase,[47,48] and the α-$NaFeO_2$-like[37,38] structure which is here referred to as the α-phase. The T- and α-phases have the same in-plane structure but differ in the relative stacking of layers, leading to the α-structure containing three ScS_2 layers in the primitive unit cell, compared to the one in the primitive unit cell of T-ScS_2. The Hc-phase has a different layer structure, and possesses two layers of ScS_2 in its primitive unit cell. To consider intercalation with the different species, supercells of $(2 \times 2 \times 2)$, $(2 \times 2 \times 1)$, and $(2 \times 2 \times 1)$ were used for the T-, Hc-, and α-phases, respectively. These supercells provided eight different intercalation sites for the T- and Hc-phases, and twelve sites for the α-phase. These allowed for various filling configurations, which were explored, the details are in the ESI† Section S1. Whilst other phases are possible for the TMDCs, such as 3R and distorted T structures, their intercalation environments are similar to that of the T-, Hc-phase, or α-phases, and so have not been explicitly considered here. It was found through two different methods (the details of which are presented in the ESI,† Section S1) that the favoured intercalation site in all three phases of ScS_2 is the octahedrally-coordinated site. Consequently, this site has been used in the following study.

All structural relaxations were completed using the Perdew–Burke–Ernzerhof (PBE)[49] functional form of the generalised gradient approximation (GGA), using the conjugate gradient algorithm and converged to a force tolerance of 0.01 eV per atom, while electronic self-consistency is considered to an accuracy of 10^{-7} eV. Of these, only the most energetically favourable structures at each level of lithium intercalation were considered. To account for the inaccurate calculation of exchange in GGA functionals, the HSE06 hybrid functional[50–52] was also used for a selection of systems. Monkhorst-Pack grids[53] of k-points equivalent to a $6 \times 6 \times 6$ grid in the supercells are used throughout.

Phonon band structures were obtained using the frozen-phonon method employed with Phonopy.[54] For these, the primitive unit cells of the pristine and intercalated structures were geometrically relaxed to a force tolerance of 0.0001 eV per atom, and electronic convergence of 10^{-8} eV. From these, the unique displacements were generated in supercells of $6 \times 6 \times 1$. Elastic properties were determined using these primitive cell for the pristine and interalated T-phase ScS_2. The elastic and internal strain tensors were computed from the second order derivatives of the total energy with respect to the position of the ions and changes to the size and shape of the unit cell, as employed in VASP. From the elastic tensor, various elastic moduli were computed, as outlined in the ESI† Section S2.

One possible method commonly used to modify the properties of electrodes is through the introduction of other elements, in particular substitution with transition metals[55–57] or lithium.[13] We consider the substitution of these metals in place of the scandium, which can be achieved through additional precursor materials. For low quantities of alternative metals this results in a substitutional doping,[4] and for higher concentrations this results in metal mixing akin to how cobalt in lithium cobalt oxide is replaced with nickel and manganese in NMC. Seeing the effects of doping and metal mixing in other materials, it offers the natural question as to whether it can be employed to enhance the properties of ScS_2. Here, we consider

the metals Co, Cr, Fe, Hf, Mn, Nb, Ni, Sn, Ta, Ti, V, and Zr for this substitution, which were chosen to ensure a sufficient spread of species from across the transition metal block. We have also considered lithium as substitutions could occur during synthesis or cycling.

Due to the number of possible concentrations (and the configurations of each of those concentrations) available for metal mixing in the α-phase, we have limited this part of our study to the T-phase. Different concentrations of substitutions were considered, with all unique configurations being considered for each concentration of mixed metals. For $Sc_{1-x}M_xS_2$, concentrations of $\frac{0}{8} \leq x \leq \frac{8}{8}$ in increments of $\frac{1}{8}$ were considered, with $x = \frac{0}{8} = 0$ corresponding to the ScS_2 composition and $x = \frac{8}{8} = 1$ corresponding to the MS_2 composition. The configurations of mixing used are equivalent to the different configurations used for lithium intercalation, with the same indexing being used for the metal species instead of the intercalated lithium. Once the $Sc_{1-x}M_xS_2$ compound is synthesised, the metal species M becomes 'locked' in the host structure due to bonding with the sulfur atoms. It is thus more difficult for the metal species to reconfigure into a lower energy configuration than it would be for intercalated species such as lithium. As such, we consider a random configuration of metal mixing by taking the average of the different configurations considered.

2.2 Methods for material evaluation

To compare ScS_2 intercalated with different amounts of a metal (M = Li, Na, K, Mg), the voltage, V, can be calculated using,[58,59]

$$\begin{aligned} V &= -\frac{\Delta G}{\Delta Q} \\ &\approx -\frac{\Delta E}{\Delta Q} \\ &= -\frac{E_{M_{x_2}ScS_2} - [E_{M_{x_1}ScS_2} + (x_2 - x_1)E_{Li}]}{(x_2 - x_1) \times ze}, \end{aligned} \quad (1)$$

with change in Gibbs free energy, ΔG, total metal content $x_2 > x_1$, E_{M_a,ScS_2} is the energy of the supercell bulk ScS_2 structure with a metal atoms per ScS_2 formula unit, and E_M is the energy of the corresponding metal atom as found in its bulk form.[60] z is the valency of the intercalant, and so $z = 1$ for Group I metals and $z = 2$ for Group II metals.

In some situations, however, taking the difference between two equivalent structures of different lithium contents does not always give the most accurate representation of what happens in reality. For example, intercalants have been found to cluster into domains for some materials rather than distributing evenly throughout the host.[61,62] In these cases, it is more accurate to consider combinations of different lithium concentrations; for example, it might be favourable for lithium to fill one cell to $LiScS_2$ and leave an adjacent cell empty, rather than filling a single cell to $Li_{0.5}ScS_2$. This would be indicative of clustering/domain separation, and so has been considered in the voltage calculation.

For the following discussion, we will use lithium (Li) as the stand-in for Group I intercalants, and magnesium (Mg) for Group II intercalants. The stability of TMDCs for lithium intercalation depends heavily on the formation of Li_2S. Generally, when this compound forms the reaction becomes difficult to reverse due to the loss of the layered structure and the required separation of the lithium and sulfur. By assessing the relative stability of the Li_2S phase against the intercalated structure, one can construct phase diagrams[63] to indicate the thermodynamic stability of the intercalated structure at different intercalant concentrations. In terms of the chemical potential, we express this limit as,

$$\Delta\mu_{Li} \leq \frac{1}{4-a}\{2\Delta H(Li_2S) - \Delta H(Li_aScS_2) + \Delta\mu_{Sc}\}, \quad (2)$$

where $\Delta H(A)$ gives the enthalpy of formation of the compound A with respect to the bulk constituents, and $\Delta\mu_B$ is given by $\Delta\mu_B = \mu_B - \mu_B^0$, with μ_B being the chemical potential of species B in Li_aScS_2, with B = Li, Sc, S. Due to the different valency between the alkali and Earth alkaline metals we consider MgS as a different conversion product for the intercalation of the Group II metals. The equivalent limit is then given as,

$$\Delta\mu_{Mg} \leq \frac{1}{2-a}\{2\Delta H(MgS) - \Delta H(Mg_aScS_2) + \Delta\mu_{Sc}\}. \quad (3)$$

Further limits can be considered on the chemical potential, which are expressed as,

$$\Delta\mu_{Li,Mg,Sc,S} \leq 0, \quad (4)$$

indicating that the system has not formed the elemental bulks, and

$$\frac{1}{a}\{\Delta H(Li_aScS_2) - \Delta H(ScS_2)\} \leq \Delta\mu_{Li}, \quad (5)$$

which indicates that the intercalated TMDC will not spontaneously deintercalate. The origins of these limits are given in the ESI,† Section S3.

3 Results

3.1 Determination of structure

We explore the phase space of $LiScS_2$ using our random structure search RAFFLE, details of which are presented in the ESI,† Section S4. Of the over 800 structures generated and structurally relaxed, the 20 lowest-energy systems are presented in Fig. 1a Of these, the eight lowest-energy systems are are all T-phase structures with hexagonal symmetry, with the differences in energy arising from different coordination of the lithium with the ScS_2 layers, relative shifts of the ScS_2 layers, and small structural fluctuations arising from the tolerances of the search. These are indicated in Fig. 1b, where the structures with octahedrally-coordinated lithium are lower in energy[23,60,62,64] than the equivalent systems with tetrahedrally-coordinated lithium due to the higher coordination between lithium and sulfur (see ESI,† Section S1). There is then a large jump of

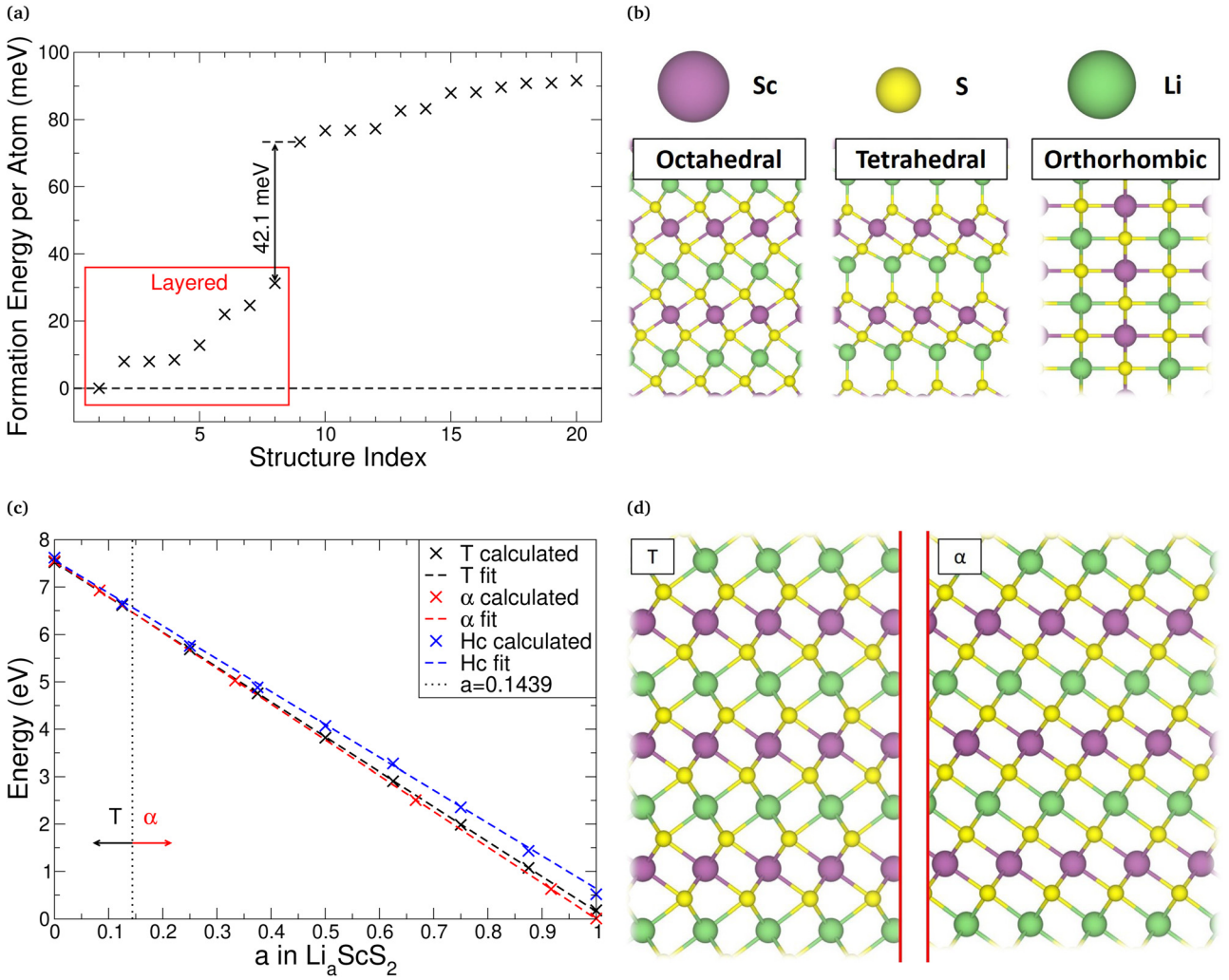

Fig. 1 (a) Resents the calculated formation energies per atom for the 20 lowest-energy structures of $LiScS_2$ found using the RAFFLE structural prediction algorithm. The results have been shifted such that the lowest-energy structure has a formation energy of 0 eV per atom. The typical structures obtained from this search are presented (b) with the layered structures having octahedral or tetrahedral coordination, and the non-layered structure being orthorhombic. (c) Shows the relative energy per formula unit for T-, α- and Hc-phases of Li_aScS_2, for a range of concentrations a. Linear fits have been presented in eachto identify the crossing points. (d) Shows the relation between the T- and α-phases of $LiScS_2$.

42.1 meV per atom to the next group of structures, which have orthorhombic unit cells. As this energy exceeds typical values associated with thermal energy, it is safe to conclude that the layered structure will preferentially form.

As the structure search shows that layered structures are the most favourable, we explicitly investigate them further. As with all partially heuristic methods of structure searching, the result is never guaranteed to be the true ground state. So, to ensure that we do not limit our investigation to the results of the random structure search, further layered polymorphs of intercalated ScS_2 were also considered. Specifically, we focused on the TMDC 1T-phase (following the results of the random structure search), the TMDC 2Hc-phase, and the α-ScS_2 phase (following experimental evidence[37,38]). The results of this are presented in Fig. 1c, where we show the energies (per formula unit) of each of the considered phases of Li_aScS_2. This allows for easy comparison of the different phases and indicates which phases are energetically preferred for different intercalation concentrations. For visual aid we have included a linear fit, which allows us to determine that the T-phase is the lowest in energy for low intercalant concentrations ($a < 0.15$ in Li_aScS_2), whereas for higher concentrations the α-phase is preferred. These two structures are presented in Fig. 1d, where the relative shift of the ScS_2 layers can be seen. We see the same results for the other intercalant species, the results of which are presented in the ESI,† Section S5. Further discussion of how the functional choice, zero-point energy and finite temperature corrections affect this ordering are discussed in the ESI,† Section S6.

To further ensure we have not missed the preferred intercalation site we have also carried out NEB calculations with a lithium intercalant, further discussion of which are in ESI,† Section S1. The results of this are shown in Fig. 2, where we have considered diffusion between two equivalent octahedral sites (Route A), between adjacent octahedral and tetrahedral

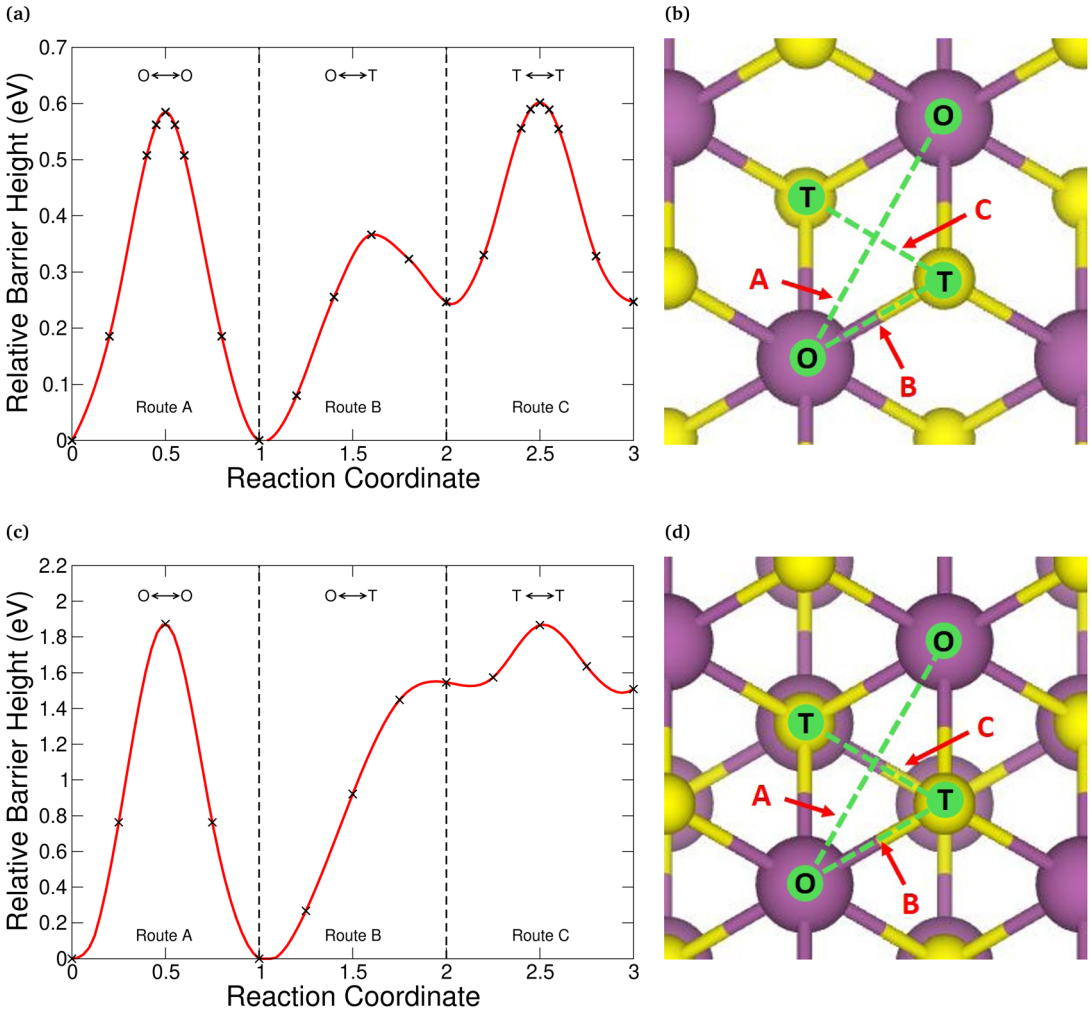

Fig. 2 Nudged elastic band results used to determine site of intercalation. (a) Shows the results for T-ScS_2 along the routes presented in (b) similarly, (c) hows the results for α-ScS_2 along the routes presented in (d). The intercalation sites these routes are between, the octahedrally coordinated (O) and tetrahedrally coordinated (T), are also indicated.

sites (Route B) and between two equivalent tetrahedral sites (Route C), and are shown in Fig. 2b for the T-phase and Fig. 2d for the α-phase. These results show that the most favourable intercalation site for each of the phases is the octahedral-coordination (O) site, which is the site of intercalation used throughout this work. This is in agreement with other TMDC investigations,[23,60,62,64] as well as the results of the structure search. These NEB results also allow us to comment on the diffusion properties of intercalants in ScS_2. As the rate of diffusion follows an Arrhenius equation, the height of the activation barriers is a key parameter for characterizing electrode materials. For both T- and α-phases we see that, whilst Route A offers the most direct path between two octahedral sites, diffusion along Route B has a lower activation energy. Route A in the T-phase demonstrates a barrier height of 0.58 eV, and 0.37 eV (0.12 eV) along Route B. These compare very well with the 0.67 eV and 0.34 eV see for lithium diffusion along monolayer T-ScS_2.[40] We see the same for the α-phase ScS_2, though we do note significantly larger barriers of 1.87 eV along Route A and 1.55 eV (0.01 eV) along Route B. These larger barriers are partially caused by the particular methods used for generating these NEB barriers. However a more significant cause is due to the relative layer shift seen for the α-phase compared to the T-phase resulting in an 'interlocking' of layers, and hence a sulfur of one layer protrudes into the void space of the next. Thus we see a larger barrier to ionic movement.

We are also interested in the structure of ScS_2 when the intercalants are removed, and so we have investigated a range of Sc–S stoichiometries to determine the stability of ScS_2. As the data available within literature and on databases such as the ICSD and Materials Project[65] for scandium-sulfide compounds is fairly limited, we have also used the structures of scandium-oxide analogues. The results of this are presented in ESI,† Section S7. For the composition ScS_2, the layered T-structure is found to be the lowest in energy, though it lies 0.37 eV above the convex hull, and a mixture of Sc_2S_3 and S would be preferred.

3.2 Properties of ScS_2 cathodes

3.2.1 Voltages. ScS_2 has several properties which are attractive as a cathode. In Fig. 3 we present the voltage, phase stability and

volume expansion of ScS_2 for Li, Na, K, and Mg intercalant ions. The voltage profiles of α-ScS_2 intercalated with the considered intercalants are presented in Fig. 3a. For ScS_2 intercalated with Group I metals, our calculations show that the voltages at low levels of intercalation reach above 4.5 V. As the concentration of the intercalant increases, the decrease in voltage across the range explored is less than 1.5 V, but remains above 3 V. The α-phase shows for Li, Na and K no change in the voltage for concentrations of $a > 0.4$. Increasing the atomic number of the Group I intercalant results in a small decrease in the average intercalation voltage. Whilst for Li intercalation the average voltage is 3.977 V, this drops to 3.874 V for Na, and to 3.799 V for K. This drop in voltage is due to the reduced charge transfer from the intercalated species to the host material, as is shown through Bader analysis (see ESI† Section S8), where the lithium charge is 0.88 $|e|$, the sodium charge is 0.85 $|e|$, and the potassium charge is 0.80 $|e|$. The voltages for the other phases of intercalated ScS_2 are presented in the ESI† Section S9. These show that there is much less variation in the voltage compared to that for the α-phase for each of the intercalated species. We also see that the voltage obtained from T-ScS_2 is about 0.3 V lower than that obtained from the equivalent α-ScS_2 structure. As the structures of the individual ScS_2 layers are the same in each of these phases, the increase in output voltage must be due to the change in bonding environment arising from the relative shift in the ScS_2 layers. However, for Li, Na and K, irrespective of phase the voltages remain above 3 V for all concentrations considered.

For magnesium intercalation the voltage behaviour is different from that of the Group I elements. The average voltage is 1.474 V for α-ScS_2, but changes considerably by 2.5 V across the range. This is due to the double valency of magnesium allowing for two changes in oxidation state of the host material. This behaviour is also present in the T- and Hc-phases. All phases, when fully intercalated ($a = 1$), decrease to voltages below 0.6 V.

It is important to make a careful choice of exchange–correlation functional in first-principles calculations, as it can lead to discrepancies in the electronic structure[66–68] and material energetics.[69–71] We compare our PBE results with those obtained from the HSE06 functional for a limited number of

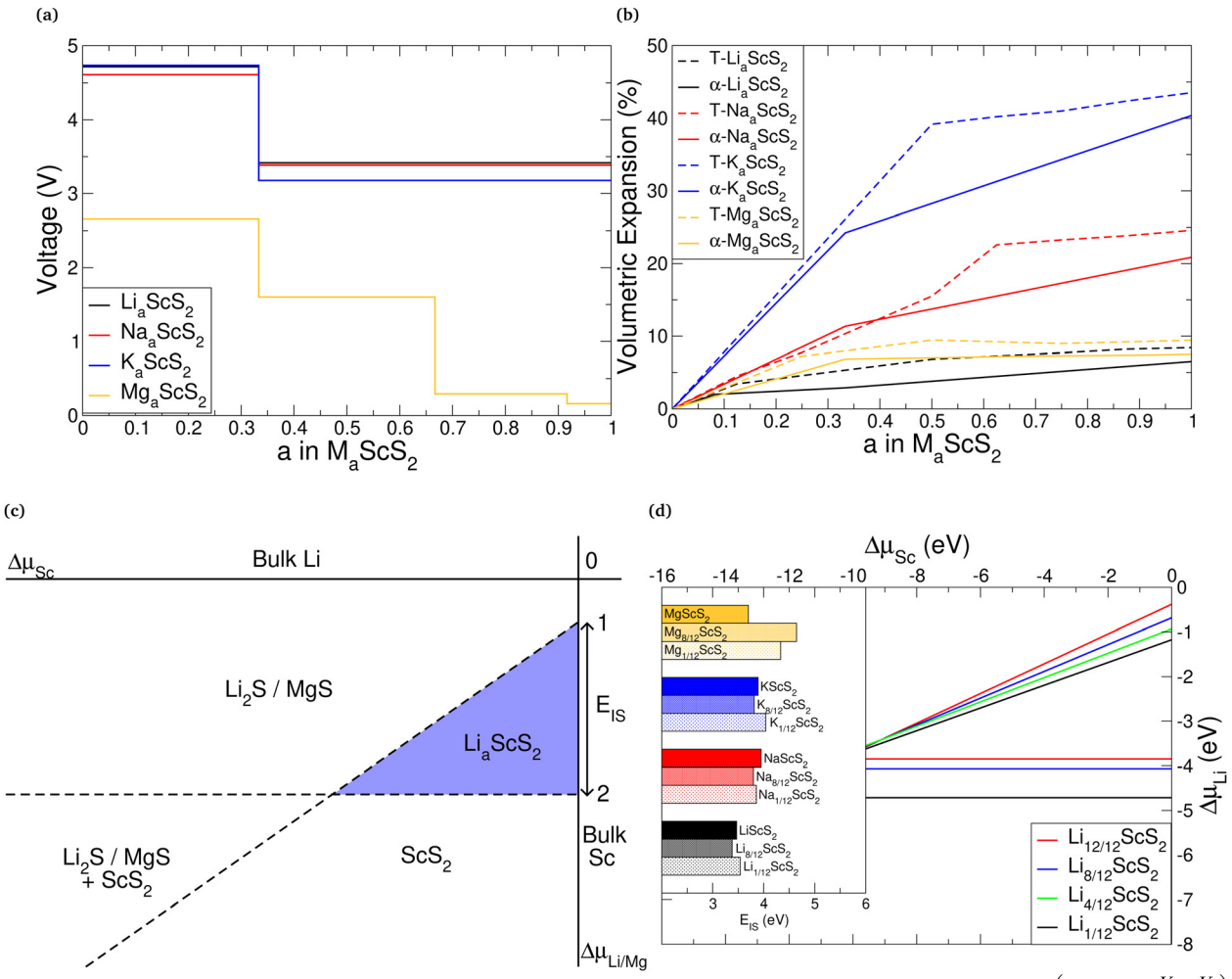

Fig. 3 (a) Resents the voltage profiles for α-ScS_2 intercalated with Li, Na, K, and Mg. (b) Shows the percentage volume change $\left(\% = 100 \times \frac{V - V_0}{V_0}\right)$ of T-ScS_2 and α-ScS_2 caused by intercalation. (c) Shows a schematic phase diagram, described by eqn (2)–(5). (d) Shows the resultant phase diagram for α-ScS_2 intercalated with different concentrations of Li, and the inset presents the the values of E_{IS} for α-ScS_2 intercalated with each of the considered intercalants.

cases (see ESI† Section S10) to determine the sensitivity of the results to functional choice. Using the hybrid functional we obtain higher voltages of 4.440 V (Li), 4.420 V (Na), 3.953 V (K), and 1.719 V (Mg). These are higher than the PBE voltages by 0.463 V, 0.546 V, 0.154 V, and 0.245 V, respectively. However, the voltage ordering is maintained and thus both functionals indicate that the ScS_2 would be very suitable for a cathode material.

3.2.2 Volumetric expansion. The volume change of ScS_2 upon cycling needs to remain suitably small for use as an intercalation electrode. Fig. 3b shows the volumetric expansion that arises in T-ScS_2 and α-ScS_2 upon intercalation. This is given as a percentage of the unintercalated bulk material volume, using $\% = 100 \times \frac{V - V_0}{V_0}$, where V_0 is the volume of the unintercalated bulk material. From the figure, we see that as the size of the intercalant is increased from Li to Na to K, the expansion increased by a larger percentage accordingly. For example, the volume change from intercalating with lithium to $LiScS_2$ is 6.51%, which is comparable to the 8% observed for NMC.[72] However, for $NaScS_2$ the expansion exceeds 20%, and for $KScS_2$ is exceeds 40%. Interestingly, intercalation with magnesium leads to a volume expansion of 7.53%, comparable to that arising from intercalation with lithium, which is due to the larger nuclear charge on the Mg resulting in a reduced ionic radius.

3.2.3 Thermodynamic stability. One can construct thermodynamic phase diagrams in terms of the chemical potentials of scandium and the intercalated species to determine the stability of the intercalated structure against undesirable conversion reactions. We use this to evaluate the capacity of the material, reasoning that the formation of Li_2S (or equivalent product) will result in irreversible loss of the layered structure and hence cyclability. A schematic of a phase diagram is shown in Fig. 3c where phase boundaries are given by eqn (2)–(5). Here, we are limited to the quadrant where the chemical potential of the intercalant species and of scandium are both negative, following eqn (4), which specifies that the elemental bulk forms of the constituent atoms do not form. The diagonal line depicts the boundary described by eqn (2) and (3), above which we would see the intercalated ScS_2 undergo conversion to scandium metal and either Li_2S or MgS. Finally, the horizontal line shows the boundary described by eqn (5), below which it is not energetically favourable for intercalation to take place, and the pristine ScS_2 would remain. The blue region satisfies eqn (2)–(5), and indicates a 'window of stability' for which the intercalated structure is stable. To quantify this window of intercalation stability, we use the quantity E_{IS}, which is the difference in the intercepts of the two boundaries with the $\Delta\mu_{Li/Mg}$ axis. An expression for this is given in the ESI,† Section S3.

The phase diagram for α-ScS_2 intercalated with Li is presented in Fig. 3d, and the resultant values of E_{IS} for each of the intercalants is presented in the inset. It is clear to see that, for the range of intercalation concentrations presented here, ScS_2 has a sizeable window of stability with E_{IS} values in excess of 3 eV. This means that ScS_2 has a total capacity of 243.99 mA h g^{-1} (487.98 mA h g^{-1}) at full intercalation for the Group I intercalants (Mg). For the Group I intercalants, E_{IS} remains relatively unchanged with intercalant concentration.

The thermodynamic stability behaviour for magnesium intercalation is different from that of the Group I intercalants. It has very favourable energetics for low intercalation, but for higher concentrations E_{IS} dramatically reduces. This arises from a significant upward shift of the phase boundary between ScS_2 and Mg_aScS_2, given by eqn (5). This behaviour is not dependent on the phase of the ScS_2. This can be seen in the ESI,† Section S3, where equivalent phase diagrams for the intercalation stability of T-ScS_2 and Hc-ScS_2 are presented and similar trends are observed.

To further validate our approach, we have compared the HSE06 and PBE functionals for this system. We see the value of E_{IS} using HSE06 is a more favourable than compared to PBE. This improvement to E_{IS} arises from a downward shift of the horizontal line described by eqn (5), and very little change in the diagonal line described by eqn (2). We see that the stability trends hold for both functionals, and that the more accurate exchange is only important for the comparison between ScS_2 and intercalated ScS_2.

3.2.4 Dynamic stability. The thermodynamic phase diagrams allowed us to determine the range of concentrations for which the intercalated materials are stable against conversion reactions. However, it is also important to assess whether these materials are dynamically stable by considering their phonon modes. Fig. 4 presents the phonon band structures for pristine α-ScS_2, and α-ScS_2 intercalated with lithium. As can be seen, the fully intercalated structure is phonon-stable. However, for bulk α-ScS_2, it is clear to see the presence of imaginary phonon modes in the Γ–M path of the Brillouin zone which result in dynamic instability. The motions associated with imaginary modes at −1.16 THz (−38.7 cm^{-1}) correspond to longitudinal in-plane oscillations of the ScS_2 sheets, as indicated in the inset of Fig. 4a. This behaviour holds for Na, K, and Mg intercalated into ScS_2. This data along with the other phases of ScS_2 considered are presented in the ESI,† Section S6.

Our results show that $LiScS_2$ is phonon stable, and at some point, as the concentration of lithium is decreased, the phonon-stability is lost. The evaluation of the phonon band structures for intermediate lithium concentrations allows us to determine the lowest concentration of lithium we can access before the intercalated layered structure becomes dynamically unstable. For the α-phase, the instability is also seen up to and including $Li_{\frac{2}{12}}ScS_2$. Similarly for T-ScS_2, $Li_{\frac{1}{8}}ScS_2$ is unstable whereas $Li_{\frac{2}{8}}ScS_2$ is not. We can therefore conclude that the lowest concentration of lithium that can be reached (corresponding to the depth of discharge and hence the maximum reversible capacity) in ScS_2 lies in the range $0.125 < a < 0.25$. Taking the range of intercalation to be $0.25 < a < 1$, corresponding to 75% of the theoretical capacity, this gives a charge capacity of 182.99 mA h g^{-1}, which is comparable to the ~200 mA h g^{-1} of other materials.[1–9] The 75% of the maximum capacity compares well with the 60–80% available in NMC materials.[5]

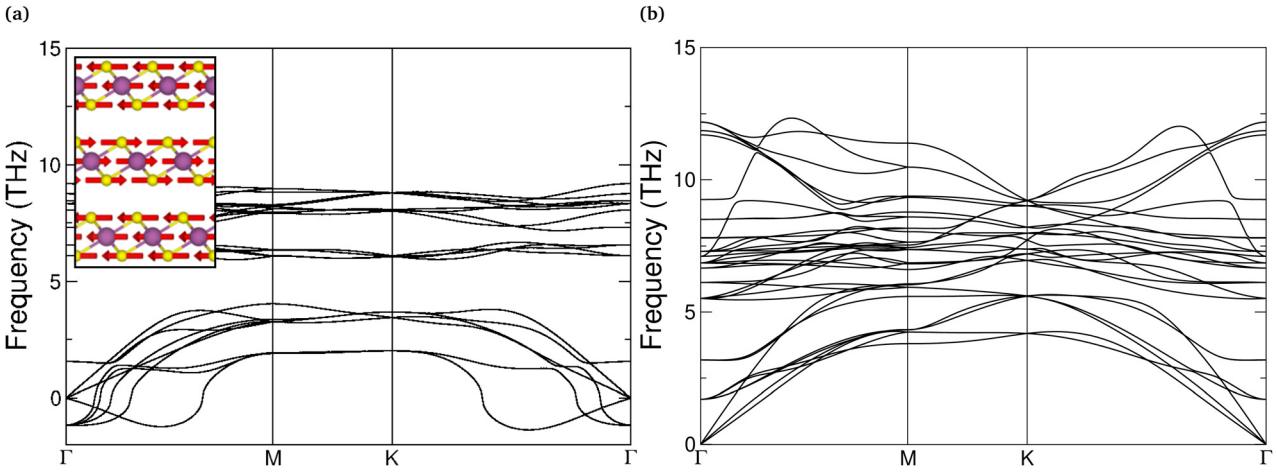

Fig. 4 Phonon band structures for α-ScS_2 and α-$LiScS_2$. (a) Shows the phonon band structure for unintercalated α-ScS_2 structure, with the inset showing the atomic structure and motions associated with the imaginary modes at Γ. (b) Shows the phonon band structure for α-ScS_2.

3.2.5 Elastic properties. For stable intercalation cycling it is desirable for the electrode material to be resistant to the associated stresses. One key metric for this is the Pugh ratio, given as the ratio of the bulk modulus and shear modulus, which can be used as an indicator of how ductile or brittle a material is. For Pugh ratios greater than 1.75 materials are usually considered ductile, whereas ratios of less than 1.75 are considered brittle. This ratio, along with other elastic properties,[72,73] for the different intercalants is shown in Fig. 5 for T-ScS_2, and further details are presented in ESI,† Section S2. With intercalation, our results show an increase in the bulk, shear and Young's moduli for ScS_2, which follows the results for intercalation of other layered materials.[74] For the Group I intercalants, as the nuclear mass increases we identify a gradual decrease in each of the elastic moduli. However, we note that magnesium intercalation results in a higher stiffness. Whilst the binding energy of Mg into ScS_2 is lower, the higher charge of the intercalant species results in significantly higher Coulomb forces and thus a stiffer system. The inset of Fig. 5 presents the Poisson ratio, and the Pugh ratio. The Poisson ratio for ScS_2 is 0.38, but drops within the range 0.21–0.25 upon intercalation. We can see that the Pugh ratio for pristine ScS_2 is 3.70, well above the 1.75 Pugh criterion, but drops below 1.75 when fully intercalated. It has been indicated previously[72,74] that the change in the elastic moduli as a function of concentration is near linear. As such, these materials remain ductile for the majority of concentrations, becoming only slightly brittle when fully intercalated. Compared to other layered materials, such as $LiCoO_2$ and graphite,[74] ScS_2 and its intercalated forms are much more ductile, and so are more attractive for use in flexible electronics.

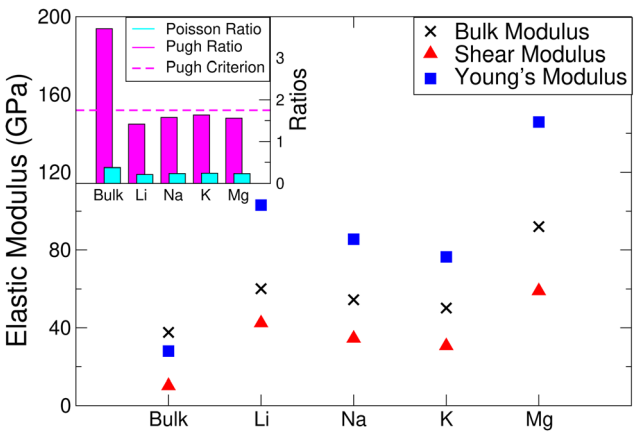

Fig. 5 Elastic properties of T-ScS_2 in its pristine and intercalated forms. The bulk and shear moduli were calculated using the Voigt scheme.

The elastic stability conditions for specific crystal types have been outlined elsewhere,[75] which have been used here to assess the stability of the T- and α-phases. We find that the elements of the elastic tensor for both T- and α-phases (see ESI,† Section S2) break the requirements of $c_{44} > 0$ and $c_{14}^2 < \frac{1}{2}c_{44}(c_{11} - c_{12}) = c_{44}c_{66}$, and so the pristine material is not elastically stable. However, each of the intercalated phases meet all of the conditions, and so are elastically stable.

3.2.6 Electronic structure. As many electrode materials require conductive additives (such as graphitic carbon) to allow for electronic conduction during cycling of a cell, determining the material electronic structure is also necessary. In the unintercalated form, as shown in Fig. 6, ScS_2 has a metallic nature with a Fermi level intersecting a band. This is seen with the other phases considered, as shown in ESI,† Section S11. The metallic nature of ScS_2 is also seen using the HSE06 functional. This is ideal for electrode materials, as it means that conductive additives are not necessary to facilitate the electron conduction. From the orbital-projected density of states, it can be seen that the valence bands of each of the phases are dominated by sulfur p-states and the conduction bands are dominated by scandium d-states.

Equivalent data for the intercalated ScS_2 structures can also be found in the ESI,† Section S11, which show that the addition of the Group I intercalants provides electrons, filling the previously unoccupied sulfur p-orbitals, shifting the Fermi level

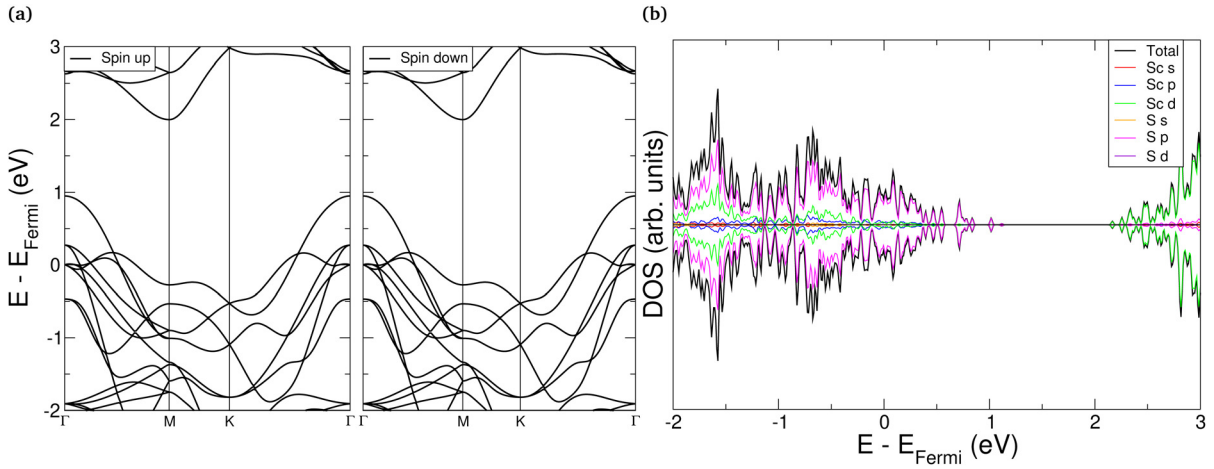

Fig. 6 Electronic band structure (a) and orbital-decomposed density of states (b) for pristine α-ScS_2. In each, all data has been normalised such that the highest occupied state (E_{Fermi}) is set to 0 eV.

(located mid-band in ScS_2) upwards. This is also shown with the charge analysis presented in the ESI,† Section S9. Upon intercalation to the point of $MScS_2$ with Group I metals, the intercalated structure develops a semiconducting nature with an occupied valence band separated from the conduction band by an moderate band gap of size ∼1 eV (PBE). Specifically for $LiScS_2$, the PBE band gap is 1.36 eV and the HSE06 Bang gap is 2.32 eV, though we note from previous work that the HSE06 functional generally overestimates the band gap of TMDC structures.[68,76] This gives a limit on the intercalation potential obtainable for practical uses: the insulating nature at this point would inhibit electronic conduction during cycling, and any intercalation past this point would require ScS_2 to be mixed with conductive additives to account for the insulating behaviour.

Magnesium intercalated into ScS_2 has different conducting behaviour compared to the group I elements, due to its double valency. Whilst the unintercalated system is conducting, intercalating to $Mg_{0.5}ScS_2$ fills the unoccupied sulfur p-orbitals and results in the structure losing its conductive nature, possessing a band gap of over 1.5 eV using the PBE functional. This would provide a practical limit during cycling, and would require conductive additives to be used to help facilitate intercalation past this point. However, past this the added magnesium provides electrons that begin to fill the unoccupied scandium d-states above the band gap.

Of the intercalant metals presented, lithium is the smallest and lightest, presents the highest (average) voltage of nearly 4 V, and has the lowest volumetric expansion. As such, lithium is identified as the best ion for ScS_2 to be used as an intercalation electrode. We summarise the key electrode properties in Table 1, along with the properties of other presently practiced electrode materials for lithium-ion batteries, where it is clear to see that ScS_2 offers a serious competitor to these materials. Below, we focus on lithium for exploring intercalation beyond the $LiScS_2$ composition, and for considering the effect of substitution of different transition metals for the scandium site in ScS_2.

3.3 Intercalation beyond $a = 1$

The intercalated $LiScS_2$ structures show both dynamic stability (with no imaginary phonon modes) and thermodynamic stability against conversion (with positive values of E_{IS}), and so the question as to the maximum possible lithium capacity still remains. As each of the octahedral sites is occupied at $LiScS_2$, any further addition of lithium results in the occupation of the tetrahedrally-coordinated sites (see ESI,† Section S1). For the supercell sizes considered, the first step of intercalation past $LiScS_2$ resulted in a stoichiometry of $Li_{\frac{13}{12}}ScS_2$. As this compound still possesses a sizeable value of E_{IS} = 3.209 eV, it is still remarkably stable against conversion reactions and demonstrates a robustness in this material to lithium intercalation beyond the usual limit considered for layered materials. However, there is a dramatic decrease in the intercalation voltage (with respect to the $LiScS_2$ structure) to 0.436 V, which indicates a clear cutoff in the practical uses for ScS_2 as a cathode material. These larger lithium contents align with the lithium

Table 1 Comparison table of key lithium-ion electrode properties for ScS_2 and other presently practiced electrode materials

Material	Voltage (V)	Intercalation capacity (mA h g^{-1})	Volume change (%)
$LiScS_2$ (this work)	3.977	182.99	6.51
$LiCoO_2$	3.9–4.7[77]	190–215[77]	3.25[78]
NMC	2.85–3.41[9]	160–189[9]	8.44[72]
$LiFePO_4$	3.5[1–3]	95,[1] 140.9,[2] 156[3]	6.81[79]
$LiMn_2O_4$	4.13, 4.25,[11] 3.9, 4.1[12]	111.5,[10] 106.3,[11] 105.2[12]	4.7[80]

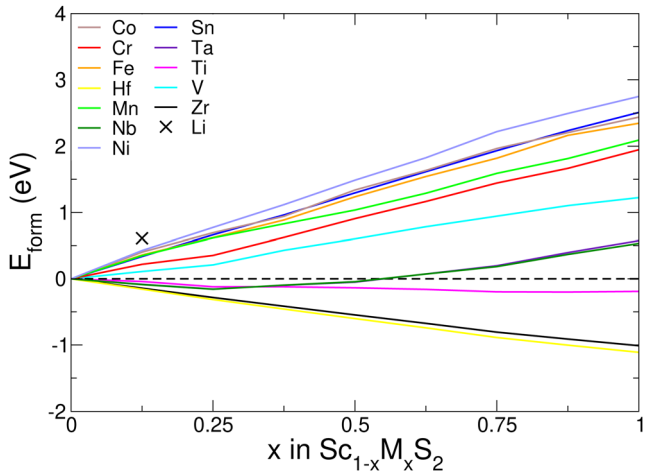

Fig. 7 Formation energy of substituting scandium with different metal species, given by eqn (6).

concentrations used in the study of monolayer ScS_2,[40] where a drop in the voltage of over 2 V was also seen for concentrations beyond $LiScS_2$.

With further intercalation we find the value of E_{IS} to drop, reaching a value of −0.735 eV at Li_2ScS_2. At these relatively high lithium concentrations the large repulsion between these positively charged ions results in the intercalated structure being destabilised and becoming more susceptible to conversion. A similar drop in E_{IS} could be expected for the monolayer system, along with further instability arising from a separation of the ScS_2 layers.

3.4 Metal mixing

One possible method commonly used to modify the properties of electrodes is through the introduction of other elements (M), in particular transition metals[55,56] or with excessive lithium,[13] resulting in the $LiSc_{1-x}M_xS_2$ compound. We first consider the formation energy of metal mixing, using,

$$E_{form} = [E(Sc_{1-x}M_xS_2) + xE(Sc)] - [E(ScS_2) + xE(M)]. \quad (6)$$

Our results, presented in Fig. 7, show that for low concentrations ($x < 0.25$), the energetic cost is very low or even negative, with lithium showing the highest formation energy of 0.61 eV at $x = 0.125$. The Group IV metals (Ti, Zr and Hf) have negative formation energies, and so it is energetically favourable to perform this substitution. We also see negative values of E_{form} for Group V elements Nb and Ta for mixing values of $x < 0.5$, whilst the other metals considered here (and $x > 0.5$ for Nb and Ta) demonstrate positive values of formation energy.

In general, our results show (see ESI,† Section S12) that there is a reduction in both the intercalation potential and the values of E_{IS} as the proportion of scandium is reduced. The exception to this is demonstrated with lithium where, for a mixing concentration of $x = 0.125$, the average voltage is increased past the 3.655 V of ScS_2 to 3.668 V. In general, the voltage and E_{IS} values for the mixed materials falls below the weighted average of the two component materials. The greatest difference from the weighted average result is most dramatically show with $Sc_{0.5}Ta_{0.5}S_2$. For voltage, the average of the two components is 2.706 V, whereas the actual voltage obtained is 2.264 V. Similarly for the value of E_{IS}, the average of the ScS_2 and TaS_2 materials is 1.857 eV, whereas the value obtained is 1.381 eV.

The energetic cost of formation of ScS_2 can be reduced by the inclusion of other metals, $Sc_{1-x}M_xS_2$. However, we see that this results in both a decrease in the obtainable voltage and a decrease in the the thermodynamic stability indicated by E_{IS}. whilst the mixing of these systems reduces the suitability of ScS_2 as a cathode, the mixing of scandium into other materials for cathodes could be highly beneficial.

4 Conclusion

In this work, we have presented a thorough first-principles study into the performance of layered ScS_2 as a potential cathode electrode material. We have applied a random structure search to demonstrate that the ground state phase for the intercalated material is a layered structure, agreeing with experimental studies and supporting its use as an electrode. From this, different layered-phases of the material were investigated and intercalated with different metal species. It was found that the T- and α-phases are energetically preferred, though they are not dynamically stable (determined through analysis of the phonon band structures) for low intercalation concentrations. The lowest achievable intercalant concentration is thus determined to be $a = 0.25$, and so a capacity corresponding to 75% of the theoretical capacity is predicted, corresponding to a charge capacity of 182.99 mA h g^{-1}.

For Group I intercalants, ScS_2 is found to have a high voltage of nearly 3.5 V which is ideal for cathodes. Whilst this is reduced to 1.5 V for intercalation with magnesium (a Group II metal), the double valency offers a larger range of charge transfer and hence a comparable energy density. This low voltage also offers some promise for an anode. Thermodynamic phase diagrams were constructed to evaluate the stability of the layered ScS_2 material against the conversion reaction forming Li_2S (or equivalent compound), a reaction commonly seen for TMDC sulfides when intercalated. ScS_2 was found to have a remarkably large window of stability, particularly when compared to the related TMDC materials. Beyond this, ScS_2 was shown to have a Fermi level which lies within a band, indicating a conductive nature that is convenient for device cycling. It also has a low volumetric expansion (below 10%) when intercalated with lithium or magnesium, something that is essential for extended device lifetime.

To explore methods that could offer some improvement to the core properties of ScS_2 material, we also considered metal mixing (substitutionally swapping out scandium atoms with transition metal elements, similar to what is done with NMC). With mixing of other metals, we find a gradual drop in both the voltage and the size of the phase diagram window of stability

which suggests that this would be detrimental to the performance of a ScS_2 electrode. However, this does highlight the potential advantage scandium could provide if mixed into other layered systems such as the layered transition metal oxides.

Our study highlights that ScS_2 shows potential as a cathode material for lithium-ion batteries, with theoretical estimates of the capacity comparable with NMC and similar materials. We hope that our study encourages further development of this material for lithium-ion batteries.

Author contributions

C. J. Price: conceptualization, data curation, formal analysis, methodology, writing – original draft, review and editing. J. Pitfield: data curation, formal analysis, methodology, writing – original draft, review and editing. E. A. D. Baker: data curation, formal analysis, writing – original draft, review and editing. S. P. Hepplestone: conceptualization, funding acquisition, supervision, writing – original draft, review and editing.

Conflicts of interest

There are no conflicts to declare.

Acknowledgements

The authors would like to acknowledge financial support from the EPSRC (United Kingdom), (Grant No. EP/L015331/1) and the Materials Chemistry Consortium, (EP/L000202, EP/R029431). The authors acknowledge the use of the University of Exeter HPC facility. We wish to acknowledge the use of the EPSRC funded Physical Sciences Data-science Service hosted by the University of Southampton and STFC under grant number EP/S020357/1.

References

1 A. S. Andersson, *Electrochem. Solid-State Lett.*, 2000, **3**, 66.
2 L. Liao, P. Zuo, Y. Ma, X. Chen, Y. An, Y. Gao and G. Yin, *Electrochim. Acta*, 2012, **60**, 269–273.
3 B. Lung-Hao Hu, F. Y. Wu, C. T. Lin, A. N. Khlobystov and L. J. Li, *Nat. Commun.*, 2013, **4**, 1–7.
4 D. Y. Wan, Z. Y. Fan, Y. X. Dong, E. Baasanjav, H.-B. Jun, B. Jin, E. M. Jin and S. M. Jeong, *J. Nanomater.*, 2018, **2018**, 1–9.
5 J. Kasnatscheew, S. Röser, M. Börner and M. Winter, *ACS Appl. Energy Mater.*, 2019, **2**, 7733–7737.
6 G. W. Nam, N. Y. Park, K. J. Park, J. Yang, J. Liu, S. C. Yoon and K.-Y. Sun, *ACS Energy Lett.*, 2019, **4**, 2995–3001.
7 W. Li, S. Lee and A. Manthiram, *Adv. Mater.*, 2020, **32**, 2002718.
8 N. D. Phillip, A. S. Westover, C. Daniel and G. M. Veith, *ACS Appl. Energy Mater.*, 2020, **3**, 1768–1774.
9 R. N. Ramesha, D. Bosubabu, M. G. Karthick Babu and K. Ramesha, *ACS Appl. Energy Mater.*, 2020, **3**, 10872–10881.
10 X. Li and Y. Xu, *Appl. Surf. Sci.*, 2007, **253**, 8592–8596.
11 X. Li, Y. Xu and C. Wang, *J. Alloys Compd.*, 2009, **479**, 310–313.
12 Y. Liu, J. Lv, Y. Fei, X. Huo and Y. Zhu, *Ionics*, 2013, **19**, 1241–1246.
13 H. Ji, J. Wu, Z. Cai, J. Liu, D. H. Kwon, H. Kim, A. Urban, J. K. Papp, E. Foley, Y. Tian, M. Balasubramanian, H. Kim, R. J. Clément, B. D. McCloskey, W. Yang and G. Ceder, *Nat. Energy*, 2020, **5**, 213–221.
14 Y. Ding, Q. Deng, C. You, Y. Xu, J. Li and B. Xiao, *Phys. Chem. Chem. Phys.*, 2020, **22**, 21208–21221.
15 V. V. Kulish, O. I. Malyi, C. Persson and P. Wu, *Phys. Chem. Chem. Phys.*, 2015, **17**, 13921–13928.
16 X. Zou, P. Xiong, J. Zhao, J. Hu, Z. Liu and Y. Xu, *Phys. Chem. Chem. Phys.*, 2017, **19**, 26495–26506.
17 D. Wang, Y. Zhao, R. Lian, D. Yang, D. Zhang, X. Meng, Y. Liu, Y. Wei and G. Chen, *J. Mater. Chem. A*, 2018, **6**, 15985–15992.
18 B. Zhou, H. Shi, R. Cao, X. Zhang and Z. Jiang, *Phys. Chem. Chem. Phys.*, 2014, **16**, 18578–18585.
19 J. Wu and G. Gao, *Phys. Chem. Chem. Phys.*, 2019, **21**, 4947–4952.
20 D. Ni, J. Shi, W. Xiong, S. Zhong, B. Xu and C. Ouyang, *Phys. Chem. Chem. Phys.*, 2019, **21**, 7406–7411.
21 M. Chhowalla, H. S. Shin, G. Eda, L.-J. Li, K. P. Loh and H. Zhang, *Nat. Chem.*, 2013, **5**, 263–275.
22 S. J. McDonnell and R. M. Wallace, *Thin Solid Films*, 2016, **616**, 482–501.
23 S. Fan, X. Zou, H. Du, L. Gan, C. Xu, W. Lv, Y. B. He, Q. H. Yang, F. Kang and J. Li, *J. Phys. Chem. C*, 2017, **121**, 13599–13605.
24 Y. Wei, J. Zheng, S. Cui, X. Song, Y. Su, W. Deng, Z. Wu, X. Wang, W. Wang, M. Rao, Y. Lin, C. Wang, K. Amine and F. Pan, *J. Am. Chem. Soc.*, 2015, **137**, 8364–8367.
25 Q. D. Chen, S. F. Yuan, J. H. Dai and Y. Song, *Phys. Chem. Chem. Phys.*, 2021, **23**, 1038–1049.
26 P. Luo and Z. Huang, *Solid State Ionics*, 2019, **338**, 20–24.
27 S. Bhuvaneswari, U. Varadaraju, R. Gopalan and R. Prakash, *Electrochim. Acta*, 2019, **301**, 342–351.
28 K. Nakajima, F. L. Souza, A. L. Freitas, A. Thron and R. H. Castro, *Chem. Mater.*, 2021, **33**, 3915–3925.
29 C. J. M. Rooymans, *Z. Anorg. Allg. Chem.*, 1961, **2**, 234–235.
30 G. Zhao, I. Muhammad, K. Suzuki, M. Hirayama and R. Kanno, *Mater. Trans.*, 2016, **57**, 1370–1373.
31 Z. Liu, H. Deng, S. Zhang, W. Hu and F. Gao, *J. Mater. Chem. A*, 2018, **6**, 3171–3180.
32 Z. Liu, H. Deng, S. Zhang, W. Hu and F. Gao, *Phys. Chem. Chem. Phys.*, 2018, **20**, 22351–22358.
33 Z. M. Xu, S. H. Bo and H. Zhu, *ACS Appl. Mater. Interfaces*, 2018, **10**, 36941–36953.
34 H. Zhang, X. Lin and Z.-K. Tang, *Solid State Commun.*, 2015, **220**, 12–16.
35 C. Ataca, H. Åžahin and S. Ciraci, *J. Phys. Chem. C*, 2012, **116**, 8983–8999.
36 J. A. Reyes-Retana and F. Cervantes-Sodi, *Sci. Rep.*, 2016, **6**, 24093.

37 M. van Dijk and C. Plug, *Mater. Res. Bull.*, 1980, **15**, 103–106.
38 L. Havlák, J. Fábry, M. Henriques and M. Dušek, *Acta Crystallogr., Sect. C: Struct, Chem*, 2015, **71**, 623–630.
39 D. Chakraborty, M. Pandey and P. Johari, *arXiv,* 2021, preprint, arXiv:2201.02268 [cond-mat.mtrl-sci], DOI: **10.48550/arXiv.2201.02268**.
40 A. Al Roman, M. M. Rahman, K. Hossain, S. Das and F. Ahmed, *Solid State Commun.*, 2022, **352**, 114828.
41 G. Kresse and J. Hafner, *Phys. Rev. B: Condens. Matter Mater. Phys.*, 1993, **47**, 558–561.
42 G. Kresse and J. Hafner, *Phys. Rev. B: Condens. Matter Mater. Phys.*, 1994, **49**, 14251–14269.
43 G. Kresse and J. Furthmüller, *Comput. Mater. Sci.*, 1996, **6**, 15–50.
44 G. Kresse and J. Furthmüller, *Phys. Rev. B: Condens. Matter Mater. Phys.*, 1996, **54**, 11169–11186.
45 P. E. Blöchl, *Phys. Rev. B: Condens. Matter Mater. Phys.*, 1994, **50**, 17953–17979.
46 S. Grimme, J. Antony, S. Ehrlich and H. Krieg, *J. Chem. Phys.*, 2010, **132**, 154104.
47 H. Katzke, P. Tolédano and W. Depmeier, *Phys. Rev. B: Condens. Matter Mater. Phys.*, 2004, **69**, 1–8.
48 J. Ribeiro-Soares, R. M. Almeida, E. B. Barros, P. T. Araujo, M. S. Dresselhaus, L. G. Cançado and A. Jorio, *Phys. Rev. B: Condens. Matter Mater. Phys.*, 2014, **90**, 115438.
49 J. P. Perdew, K. Burke and M. Ernzerhof, *Phys. Rev. Lett.*, 1996, **77**, 3865–3868.
50 J. Heyd, G. E. Scuseria and M. Ernzerhof, *J. Chem. Phys.*, 2003, **118**, 8207–8215.
51 J. Heyd, G. E. Scuseria and M. Ernzerhof, Erratum: Hybrid functionals based on a screened Coulomb potential, *J. Chem. Phys.*, 2003, **118**, 8207, DOI: **10.1063/1.2204597**.
52 J. Paier, M. Marsman, K. Hummer, G. Kresse, I. C. Gerber and J. G. Angyán, *J. Chem. Phys.*, 2006, **124**, 154709.
53 H. J. Monkhorst and J. D. Pack, *Phys. Rev. B: Condens. Matter Mater. Phys.*, 1976, **13**, 5188–5192.
54 A. Togo and I. Tanaka, *Scr. Mater.*, 2015, **108**, 1–5.
55 A. Bhaskar, D. Mikhailova, N. Kiziltas-Yavuz, K. Nikolowski, S. Oswald, N. N. Bramnik and H. Ehrenberg, *Prog. Solid State Chem.*, 2014, **42**, 128–148.
56 H. H. Sun, U. H. Kim, J. H. Park, S. W. Park, D. H. Seo, A. Heller, C. B. Mullins, C. S. Yoon and Y. K. Sun, *Nat. Commun.*, 2021, **12**, 1–11.
57 P. Wen, H. Wang, X. Wang, H. Wang, Y. Bai and Z. Yang, *Phys. Chem. Chem. Phys.*, 2022, **24**, 14877–14885.
58 M. K. Aydinol, A. F. Kohan, G. Ceder, K. Cho and J. Joannopoulos, *Phys. Rev. B: Condens. Matter Mater. Phys.*, 1997, **56**, 1354–1365.
59 M. Mayo, K. J. Griffith, C. J. Pickard and A. J. Morris, *Chem. Mater.*, 2016, **28**, 2011–2021.
60 A. N. Enyashin and G. Seifert, *Comput. Theor. Chem.*, 2012, **999**, 13–20.
61 Q. Zhang, R. Li, M. Zhang, B. Zhang and X. Gou, *Electrochim. Acta*, 2014, **115**, 425–433.
62 P. Gao, L. Wang, Y. Y. Zhang, Y. Huang, L. Liao, P. Sutter, K. Liu, D. Yu and E. G. Wang, *Nano Lett.*, 2016, **16**, 5582–5588.
63 Y. Koyama, H. Arai, I. Tanaka, Y. Uchimoto and Z. Ogumi, *J. Mater. Chem. A*, 2014, **2**, 11235–11245.
64 Z. Liu, H. Deng and P. P. Mukherjee, *ACS Appl. Mater. Interfaces*, 2015, **7**, 4000–4009.
65 A. Jain, S. P. Ong, G. Hautier, W. Chen, W. D. Richards, S. Dacek, S. Cholia, D. Gunter, D. Skinner, G. Ceder and K. A. Persson, *APL Mater.*, 2013, **1**, 011002.
66 B. Amin, N. Singh and U. Schwingenschlögl, *Phys. Rev. B: Condens. Matter Mater. Phys.*, 2015, **92**, 1–6.
67 F. Khan, M. Idrees, C. Nguyen, I. Ahmad and B. Amin, *RSC Adv.*, 2020, **10**, 24683–24690.
68 F. H. Davies, C. J. Price, N. T. Taylor, S. G. Davies and S. P. Hepplestone, *Phys. Rev. B: Condens. Matter Mater. Phys.*, 2021, **103**, 1–10.
69 F. Zhou, M. Cococcioni, C. A. Marianetti, D. Morgan and G. Ceder, *Phys. Rev. B: Condens. Matter Mater. Phys.*, 2004, **70**, 1–8.
70 F. Zhou, C. A. Marianetti, M. Cococcioni, D. Morgan and G. Ceder, *Phys. Rev. B: Condens. Matter Mater. Phys.*, 2004, **69**, 1–4.
71 V. L. Chevrier, S. P. Ong, R. Armiento, M. K. Chan and G. Ceder, *Phys. Rev. B: Condens. Matter Mater. Phys.*, 2010, **82**, 1–11.
72 M. Woodcox, R. Shepard and M. Smeu, *J. Power Sources*, 2021, **516**, 230620.
73 S. Shang, Y. Wang, P. Guan, W. Y. Wang, H. Fang, T. Anderson and Z.-K. Liu, *J. Mater. Chem. A*, 2015, **3**, 8002–8014.
74 Y. Qi, L. G. Hector, C. James and K. J. Kim, *J. Electrochem. Soc.*, 2014, **161**, F3010–F3018.
75 F. Mouhat and F.-X. Coudert, *Phys. Rev. B: Condens. Matter Mater. Phys.*, 2014, **90**, 224104.
76 E. A. D. Baker, J. Pitfield, C. J. Price and S. P. Hepplestone, *J. Phys.: Condens. Matter*, 2022, **34**, 375001.
77 Y. Lyu, X. Wu, K. Wang, Z. Feng, T. Cheng, Y. Liu, M. Wang, R. Chen, L. Xu, J. Zhou, Y. Lu and B. Guo, *Adv. Energy Mater.*, 2021, **11**, 2000982.
78 J. Luo, C. Dai, Z. Wang, K. Liu, W. Mao, D. Fang and X. Chen, *Measurement*, 2016, **94**, 759–770.
79 A. Yamada, S. C. Chung and K. Hinokuma, *J. Electrochem. Soc.*, 2001, **148**, A224.
80 J. Barker, *Electrochim. Acta*, 1999, **45**, 235–242.

